Load sharing in tungsten fiber reinforced Kanthal composites

B. Clausen [a,*], Mark A.M. Bourke [b], Donald W. Brown [b], E. Üstündag [c]

[a] *Los Alamos National Laboratory, LANSCE-12, P.O. Box 1663, MS H805, Los Alamos, NM 87545, USA*
[b] *Los Alamos National Laboratory, MST-8, P.O. Box 1663, MS H805, Los Alamos, NM 87545, USA*
[c] *California Institute of Technology, Keck Laboratory, M/C 138-78, 1200 E. California Blvd., Pasadena, CA 91125, USA*

Abstract

The load sharing in three tungsten fiber reinforced Kanthal matrix composites (with fiber volume fractions of 10, 20 and 30%) have been determined using in situ neutron diffraction measurements. The expected iso-strain region was limited in the 20 and 30% composites due to thermal residual stresses. The experimental data have been used to validate the predictions of a unit-cell finite element model. The model was able to accurately predict the measured in situ loading data for all three composites using the same material properties for all calculations.
© 2005 Elsevier B.V. All rights reserved.

Keywords: Metal matrix composite; Neutron diffraction; Finite element modeling; Material properties

1. Introduction

Neutron diffraction has been used extensively to measure the in situ properties of monolithic materials [1–3] and composites [4–8] as the technique provides phase specific information about the internal elastic strains in crystalline phases. The technique is capable of providing information about the anisotropy of the phases by employing single peak fitting to the diffraction peaks [1–3], but is also capable of yielding an average phase specific strain utilizing the Rietveld full pattern analysis [4–9]. The Kanthal/Tungsten composites investigated in the present work were previously the subject of a thermal residual strain study, also using neutron diffraction and finite element modeling [10]. Good agreement between the measured and predicted thermal residual strains was found using literature material parameters for both phases. In the present study, we extend the model validation to include the load sharing in the composites during tensile loading. The thermal stresses and strains developing in the cooling cycle are nominally hydrostatic in nature, and the change in loading path to the uniaxial deformation in the tensile loading cycle provides a more rigorous validation of the model capabilities.

2. Samples

As described in Ref. [10], the Kanthal/Tungsten composites were proposed as a model system for high temperature structural applications, initially investigated in collaboration between NASA Lewis and Tuft University. In the present study, we have examined the load sharing during room temperature tensile testing of three of these composites—with fiber volume fraction of 10, 20 and 30%. The Kanthal matrix composition was 73.2 wt% Fe–21 wt% Cr–5.8 wt% Al–0.04 wt% C [20]. Tapes containing unidirectional fibers were produced at 1065 °C by the arcspray method. The tapes were then hot pressed at 1065 °C for 1 h before being cooled to room temperature. The as-fabricated bars were approximately 25 mm wide, 2.5 mm thick and 200 mm long. Tensile test samples with a gauge width of 12 mm were cut from the bars. As seen in Fig. 1, the distance between layers is fairly uniform, but the stacking sequence is a mixture of both cubic and hexagonal stacking.

3. Neutron diffraction measurements

The in situ loading neutron diffraction measurements for the Kanthal/Tungsten composites were performed at the neutron powder diffractometer (NPD) [11] at Los Alamos Neutron Science Center (LANSCE). Fig. 2 shows a schematic of the experimental setup for the NPD diffractometer with the sample arranged at 45° to the incident beam and simultaneously measurements of diffraction patterns longitudinal and transverse to the loading direction at plus and minus 90° to the incident beam. The detector coverage on NPD is ±5.5° both horizontally and vertically. LANSCE is a spallation neutron source and the use of the time-of-flight technique enables collection of full diffraction patterns from about 0.4 to 4 Å on NPD. The data was analyzed

---

* Corresponding author. Tel.: +1 505 667 2944; fax: +1 505 665 2676.
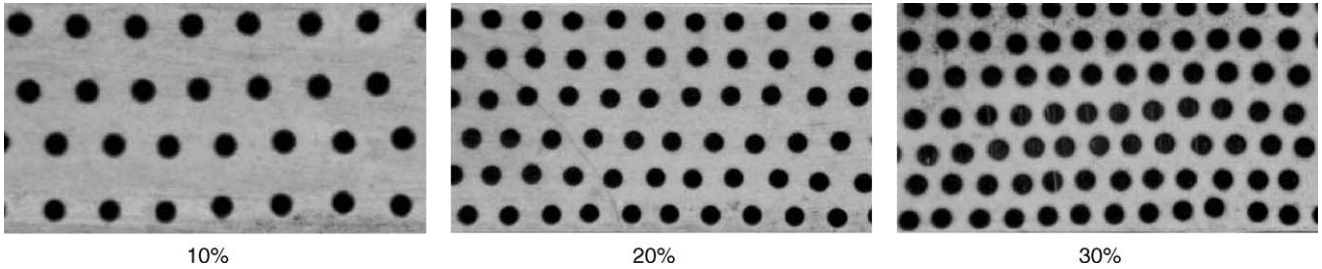*E-mail address:* clausen@lanl.gov (B. Clausen).

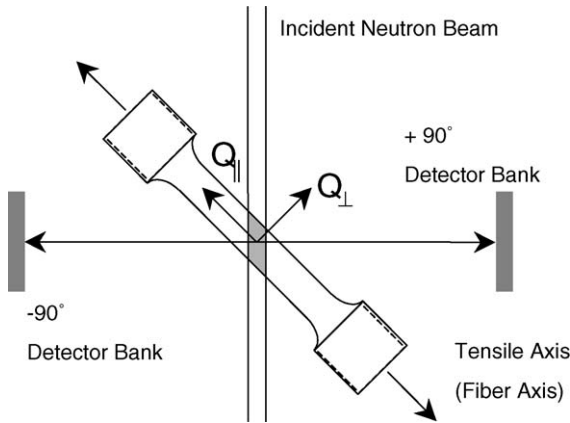Fig. 1. Fiber stacking in the composites: dark circles are the tungsten fibers.

Fig. 2. Schematic of the NPD setup. The sample orientation at 45° to the incident beam allows for simultaneous measurement of longitudinal (−90° bank) and transverse (+90° bank) strains.

with the full pattern Rietveld refinement method [12] using the General Structure Analysis System (GSAS) [13] software package to obtain elastic phase strains based on the changes in lattice parameter. The crystal structure of both Kanthal and Tungsten is body centered cubic (bcc, space group $Im\bar{3}m$) and the phase average lattice strains are calculated directly from the change in lattice parameter, a, as shown in Eq. (1).

$$\varepsilon_{\text{lattice}} = \frac{\Delta a}{a_0} = \frac{a}{a_0} - 1 \qquad (1)$$

Following the normal error propagation rules [14,15], the standard deviation of the calculated lattice strain, $\sigma_{\varepsilon_{\text{lattice}}}$, based upon the refinement can be found as:

$$\sigma_{\varepsilon_{\text{lattice}}} = \sqrt{\frac{1}{a_0^2}\sigma_a^2 + \frac{a_0^2}{a^4}\sigma_{a_0}^2} \qquad (2)$$

where σ_a is the standard deviation of the lattice parameter from the refinement and σ_{a_0} is the standard deviation of the reference lattice parameter from the refinement. In the loading measurements, the reference lattice parameter, a_0, was measured at a nominal load of 10 MPa. This small applied load is necessary to ensure that the sample is taught in the grips, as any sample movement upon loading will result in apparent strains due to the change in diffraction geometry. The refinement error bars for the measured elastic lattice strains vary slightly with fiber volume fraction, but are generally within ±25–75 $\mu\varepsilon$ (microstrain, i.e. 10^{-6}). As seen from the diffraction patterns, Fig. 3, the tungsten fibers are clearly textured; only $hh0$ peaks are present in the longitudinal diffraction pattern, indicative of a strong 110 fiber texture from the wire drawing.

4. Finite element modeling

The finite element modeling (FEM) was performed using the commercially available software package ABAQUS, Version 6.3 [16]. The model was constructed in full 3D due to the
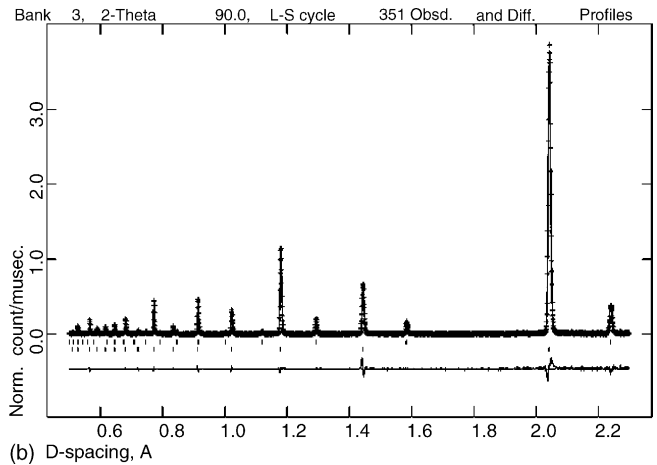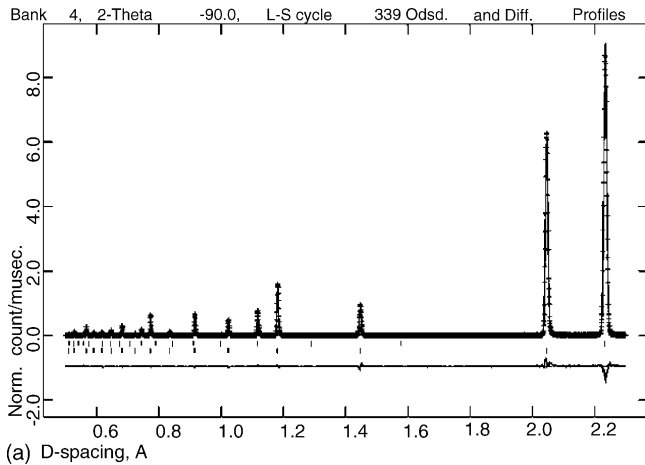

Fig. 3. Longitudinal (a) and transverse (b) diffraction patterns for the Kanthal 20% Tungsten composite. The crosses are the measured data; the line is the Rietveld refinement. The difference curve is shown below the tick marks. Upper row of tick marks are tungsten and the lower row are Kanthal. The longitudinal pattern only shows $hh0$ type tungsten peaks due to the strong 110 fiber texture developed during the wire drawing of the fibers.
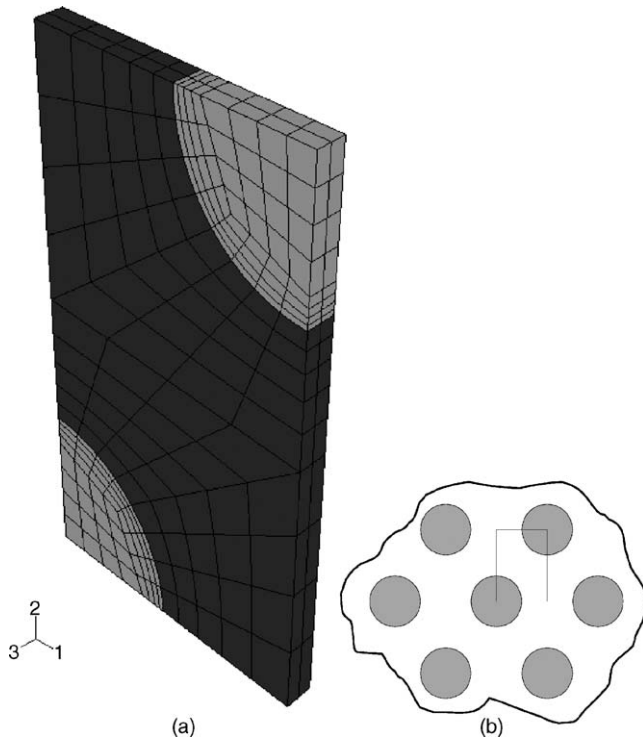
Fig. 4. The mesh in the FEM calculations for the 20% composite (a). Description of the unit-cell assuming hexagonal stacking of the fibers (b).

presented in [10]. Creep properties for the two materials are not available; hence we did not consider a viscoelastic–viscoplastic analysis. Instead, we assumed a stress-free (or freezing) temperature of 650 °C (the processing temperature was 1065 °C) and used an elastic–plastic analysis. The value of 650 °C was taken from previously reported results [10,17,18]. It is also consistent with the work of Kroupa and Neu [19] who showed, using the Bodner–Partom model, that a bilinear elastic–plastic FEM analysis could predict comparable residual stresses (in a titanium matrix composite) with a viscoelastic–viscoplastic analysis provided that the stress-free temperature was about 0.7–0.8 times the absolute processing temperature. Both materials are assumed to behave elastic-perfectly plastic, and only the yield point is given as a function of temperature in Table 1. The FEM model is a unit-cell model, and as such, the boundary conditions on the outer surfaces are taken to be symmetry boundary conditions (no movement of nodes perpendicular to the surface and no nodal rotations around directions within the surface). The symmetry boundary conditions are also employed on the surface perpendicular to the fiber axis, effectively making the mode a plane strain model. It is not possible to utilize a 2D plane strain model, as the 2D model does not allow for applying loading in the "out of plane" direction, which is needed to load the fiber composite along the fiber axis. As the strains in the fiber axis direction are constant due to the applied boundary conditions, we made the model thin and only used two layers of elements in that direction, see Fig. 4.

To be able to make a direct comparison with the neutron diffraction measurements average elastic strains for each phase have been calculated as shown in Eq. (3):

$$\bar{\varepsilon}_{kl} = \frac{\sum_i \varepsilon_{kl}^i \cdot V^i}{\sum_i V^i} \tag{3}$$

where ε_{kl}^i is the strain component in the ith element as given by ABAQUS and V^i is the volume of the ith element. The model calculations include the thermal cycle simulating the cooling of the composites from the stress-free temperature of 650 °C, but the calculated elastic strains presented below are relative to the strains calculated at an applied load of 10 MPa to mimic the experimental conditions.

requirement of loading along the fiber direction. The geometry was modeled using 20 node second order brick elements with reduced integration points [16] to enable accurate representation of the cylindrical fibers, see Fig. 4.

Previous work to determine the thermal residual strains in the composites [10] utilized cubic stacking of the fibers, but in the present work hexagonal stacking was assumed. As seen in Fig. 1, a mixture of cubic and hexagonal stacking of the fibers is observed in all the composites. The material parameters used in the present finite element calculations, the same as used in [10], are given in Table 1 and the only source of discrepancy between the model used in [10] and the current model is the fiber stacking, which results in differences of less than $\pm 150\,\mu\varepsilon$ compared to the calculated thermal residual strains

Table 1
Material parameters for Tungsten and Kanthal used in the finite element calculations [10]

| Material	Temperature (°C)	Young's modulus (GPa)	Poisson's ratio (−)	Yield stress (MPa)	Coefficient of thermal expansion (10^{-6}/°C)
Tungsten	26	395	0.28	1305	4.40
Tungsten	138	394	0.28	1179	4.42
Tungsten	251	393	0.28	1054	4.44
Tungsten	420	389	0.28	893	4.47
Tungsten	533	386	0.28	777	4.49
Tungsten	1000	360	0.28	550	4.56
Kanthal	26	202	0.28	530	9.58
Kanthal	138	196	0.28	520	9.68
Kanthal	251	183	0.28	465	10.08
Kanthal	420	172	0.28	375	10.80
Kanthal	533	162	0.28	275	11.38
Kanthal	1000	125	0.28	27	14.75
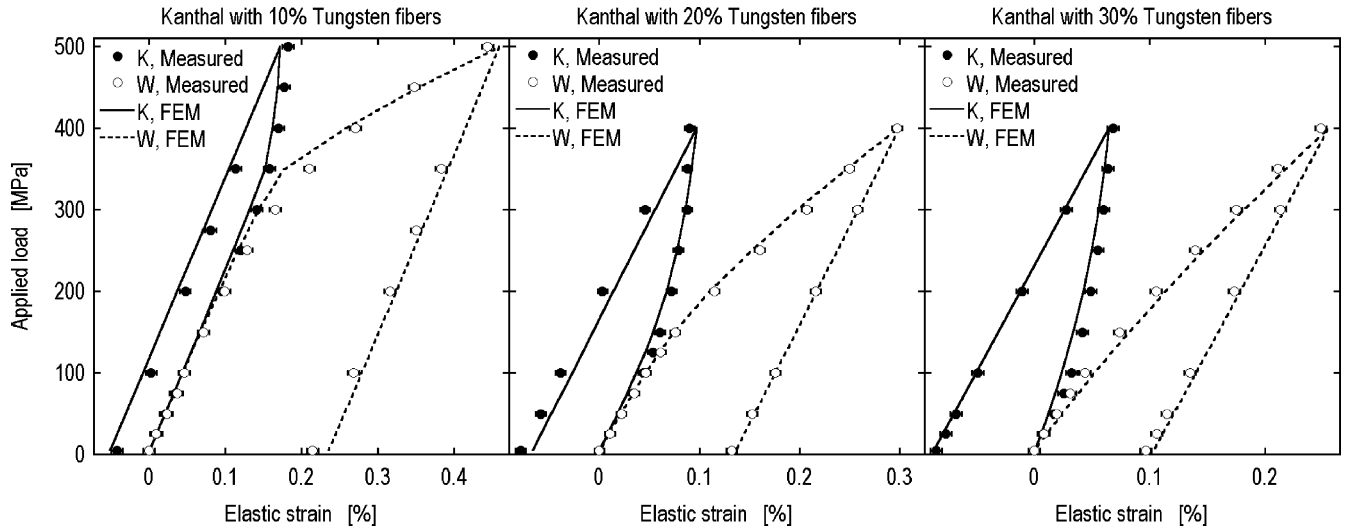
Fig. 5. Measured and calculated longitudinal elastic strain curves for the Kanthal composites with tungsten fibers. W and K denote Tungsten and Kanthal, respectively.

5. Results

The neutron diffraction measurements of internal phase strains during tensile loading have been used to validate the finite element model calculations using literature material properties for both Kanthal matrix and tungsten fibers. In the following, we have plotted the measured and calculated elastic phase strain versus the applied load to create "elastic stress–strain curves" that resemble normal macroscopic stress–strain curves. The longitudinal data is shown in Fig. 5 and the transverse data is shown in Fig. 6.

In a continuous fiber composite, an initial region of iso-strain is expected due to the geometrical constraints, i.e. the longitudinal strains would be equal in fiber and matrix. Even though a small amount of plastic deformation is observed after the thermal step in the matrix close to the fibers of the 10% composite it also shows an iso-strain region as seen in Fig. 5. The 20% composite shows a smaller iso-strain region, but in the 30% composite the matrix and fiber strains deviate from the start.

The splitting of the phase strains indicates that the yield point of one of the phases, in this case the matrix, has been reached, and then the yielding phase sheds some of its load to the phase that is still elastic. Generally, the FEM calculations for longitudinal direction are within the error bars (± 25–$75\,\mu\varepsilon$), except for the yield region of the 10% composite. It is worth noting that the elastic strain development in the matrix for all three composites virtually stops once yielding has occurred, which is in good agreement with the assumption of elastic-perfectly plastic matrix behavior. The end of the iso-strain region should be directly linked to the thermal residual stresses in the composites, and in Table 2 we have shown the measured and calculated thermal residual stresses in the composites, σ^{TRS}, together with the load level at which the iso-strain region ends, σ^{Lim}. The error bar cited for σ^{Lim} is equal to the step-size of the load between the neutron diffraction measurements. The sum of the thermal residual stress and σ^{Lim} should be approximately equal to the yield stress of the Kanthal matrix. From Table 2, it is seen that the sum of σ^{TRS} and σ^{Lim} is approximately the same as the Kanthal yield
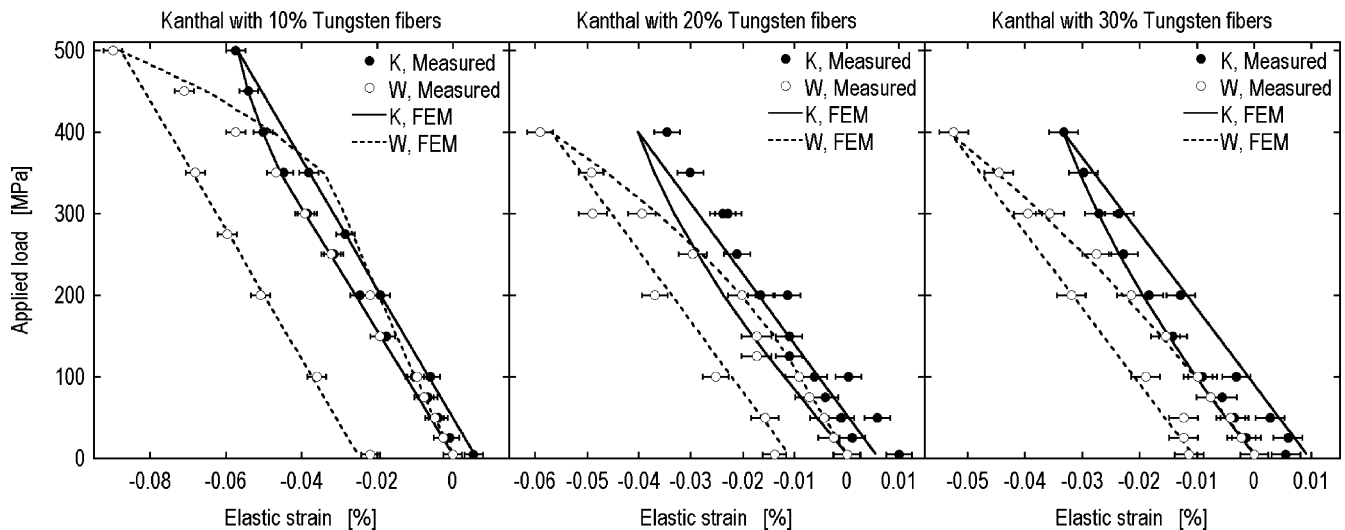

Fig. 6. Measured and calculated transverse elastic strain curves for the Kanthal composites with tungsten fibers. W and K denote Tungsten and Kanthal, respectively.

stress of 530 MPa. The values including the calculated thermal residual stresses are consistently 15% lower than the yield limit. The values with the measured thermal residual stresses for the 20 and 30% composite are well within the error bars, but the 10% composite is about 45% too low which may be due to an experimental error, as described in [10]. In the transverse direction, the finite element model predicts some splitting between the phases from the start, see Fig. 6, which is not observed in the measurements. This may be due to the averaging of the elastic strains; in the longitudinal direction the strain is fairly uniform over the entire cross-section (within each phase), but in the transverse direction it is very heterogeneous.

6. Conclusions

The neutron diffraction measurements clearly show the effect of the thermal residual stresses on the tensile yield point of the three composites, e.g. the 30% composite does not have an elastic region as macroscopic plasticity occurs immediately upon loading. The neutron diffraction measurements have been used to validate the predictions of a unit-cell finite element model of internal strains in the tungsten fiber reinforced Kanthal matrix composites. The present model validation utilized both the thermal residual strains present in the composites after manufacture and the development of internal strains due to applied tensile load. The model was able to accurately predict the in situ loading strains for the 10, 20 and 30% composites using the same material properties for the two phases for all fiber volume fractions. The model correctly predicted the limited iso-strain region in the 20 and 30% composites and was also able to correctly predict the residual phase strains in the composites after deformation. It is important to note that the model was able to predict the development of elastic strains in both matrix and fibers for a load path change, i.e. from the semi-hydrostatic stress and strain fields developed during cooling to the uniaxial stress and strain fields of the tensile loading.

References

[1] B. Clausen, T. Lorentzen, M.A.M. Bourke, M.R. Daymond, Mater. Sci. Eng. A 259 (1999) 17–24.
[2] J.W.L. Pang, T.M. Holden, P.A. Turner, T.E. Mason, Acta Mater. 47 (2) (1999) 373–383.
[3] M.R. Daymond, C.N. Tomé, M.A.M. Bourke, Acta Mater. 48 (2000) 553–564.
[4] M.R. Daymond, H.G. Priesmeyer, Acta Mater. 50 (2002) 1613–1626.

Table 2
Measured and calculated thermal residual stresses, and the observed limit of iso-strain as seen in Fig. 5

Fiber volume fraction	10%				20%				30%			
Phase	Kanthal		Tungsten		Kanthal		Tungsten		Kanthal		Tungsten	
Applied load at observed end of iso-strain (σ^{Lim}) in MPa	250±50				100±25				25±25			
Direction	L	T	L	T	L	T	L	T	L	T	L	T
Measured σ^{TRS} in MPa (±100 MPa error bar) [10]	33	−76	−2005	−878	372	126	−1632	−723	543	235	−1342	−629
Calculated σ^{TRS} in MPa	202	55	−1802	−497	365	100	−1447	−399	446	127	−1032	−295
Sum of σ^{Lim} and calculated σ^{TRS} for Kanthal, L	452±50				465±25				471±25			
Sum of σ^{Lim} and measured σ^{TRS} for Kanthal, L	283±150				472±150				568±150			

L and T denoted longitudinal and transverse, respectively.

[5] M.R. Daymond, C. Lund, M.A.M. Bourke And, D.C. Dunand, Metall. Mater. Trans. A 30 (11) (1999) 2989–2997.

[6] P. Agrawal, K. Conlon, K.J. Bowman, C.T. Sun, F.R. Cichocki Jr., K.P. Trumble, Acta Mater. 51 (2003) 1143–1156.

[7] D. Dragoi, E. Üstündag, B. Clausen, M.A.M. Bourke, Scr. Mater. 45 (2001) 245–252.

[8] D. Mari, A.D. Krawitz, J.W. Richardson, W. Benoit, Mater. Sci. Eng. A 209 (1996) 197–205.

[9] B. Clausen, S.-Y. Lee, E. Üstündag, C.C. Aydiner, R.D. Conner And, M.A.M. Bourke, Scr. Mater. 49 (2003) 123–128.

[10] P. Rangaswamy, I.J. Beyerlein, M.A.M. Bourke, M.B. Prime, A.K. Saigal, T.O. Williams, Philos. Mag. 83 (19) (2003) 2267–2292.

[11] M.A.M. Bourke, J.A. Goldstone, R.A. Robinson, Phys. B 213–214 (1995) 806–808.

[12] H.M. Rietveld, Acta Cryst. 22 (1967) 151.

[13] R.B. Von Dreele, J.D. Jorgensen, C.G. Windsor, J. Appl. Cryst. 15 (1982) 581–589.

[14] P.R. Bevington (Ed.), Data Reduction and Error Analysis for the Physical Sciences, McGraw-Hill, New York, 1969, pp. 58–64.

[15] M. Abramowitz, I.A. Stegun (Eds.), Handbook of Mathematical Functions with Formulas, Graphs, and Mathematical Tables, Ninth Printing, Dover, New York, 1972, p. 14.

[16] ABAQUS Analysis User's Manual, Version 6.3, ABAQUS, Inc., Providence, RI, 2002.

[17] A. Saigal, G.G. Leisk, S.T. Misture, C.R. Hubbard, Scr. Mater. 34 (8) (1996) 1309–1313.

[18] A. Saigal, G.C. Leisk, Mater. Sci. Eng. A237 (1997) 65–71.

[19] J.L. Kroupa, R.W. Neu, Compos. Eng. 4 (9) (1994) 965–977.

[20] C.T. Liu, V.K. Sikka, C.G. McKamey, Technical Memorandum ORNL/TM-12199, Oak Ridge National Laboratory, 1993.